Materials Research. 2013; 16(2): 453-467
DOI: 10.1590/S1516-14392012005000178

Evaluation of Properties and FEM Model of the Friction Welded Mild Steel-Al6061-Alumina

Hazman Seli*[a], *Mokhtar Awang*[b], *Ahmad Izani Md. Ismail*[c], *Endri Rachman*[d], *Zainal Arifin Ahmad*[e]

[a]*Faculty of Computer and Mathematical Sciences, Universiti Teknologi MARA Sarawak, 94300 Kota Samarahan, Sarawak, Malaysia*
[b]*Mechanical Engineering Department, Universiti Teknologi PETRONAS, Seri Iskandar, 31750 Perak, Malaysia*
[c]*School of Mathematical Sciences, USM, Penang, Malaysia*
[d]*Collaborative Microelectonic Design Excellence Centre – CEDEC, USM Engineering Campus, 14300 Nibong Tebal, Pulau Pinang*
[e]*School of Materials & Mineral Resources Engineering, USM Engineering Campus, Penang, Malaysia*

Received: February 23, 2012; Revised: September 17, 2012

Evaluation of mechanical and interfacial properties of friction welded alumina-mild steel rods with the use of Al6061 sheet are presented in this work. SEM, EDX analysis, hardness and bending strength tests were conducted. The bonds were attained through interfacial interlocking and intermetalllic phase formation with average bending strengths in the range of 40 to 200 MPa and insignificant hardness change in the parent alumina and mild steel. A preliminary simulation was made to predict the deformation, stress, strain and temperature distribution during the joining operation using a fully coupled thermo-mechanical FE model. The aluminum alloy metal being rubbed was simulated using a phenomenological Johnson-Cook viscoplasticity material model, which suited for materials subjected to large strains, high strain rates and high temperatures. The highest stress, strain and deformation are found to be within the heat affected zone of the weld close to the periphery rubbing surface region and correspond to the highest temperature profiles observed.

Keywords: *friction welding, intermetallic, FE model, interface, bending strength*

1. Introduction

Due to low density, high strength, and excellent high temperature resistance, ceramics are widely used in areas of aerospace and metallurgy. Ceramics and ceramic matrix composites possess more advantages than metals, particularly in high temperature applications. However, ceramics have low toughness which makes it difficult for used in the production of complex parts. A practical solution for this problem would be to manufacture composite parts of ceramics and metals using the joining technique to meet the requirements[1,2]. Several ceramic and metal joining techniques have been developed[3] such as mechanical joining, adhesive joining, brazing, diffusion bonding and etc. The joining of ceramics to metallic materials by means of friction welding (FW) is possible and has been successfully performed[4,5]. Friction welding is a solid-state joining process and one of the most effective processes for joining similar and dissimilar materials with high joint integrity through the combined effects of pressure and relative motion of the two workpieces, heating of the joint interface and inducing of plastic deformation of the material. Under normal conditions, the maximum temperature at the interface is just below the melting temperature[6]. The problems concerning friction welding of dissimilar materials are not only associated with their individual properties such as hardness and melting point, but also with the reactions that take place at the interface. Metals in general have a higher thermal expansion coefficient than ceramics. Therefore, when joining ceramics to metals using friction welding, very large thermal stresses will be induced and in many cases these large stresses cause joint failure. In order to overcome this problem, solid phase bonding processes have been developed in which a metallic or a composite metal–ceramic interlayer is placed between the ceramic and metal surfaces to be joined. Ceramic–metal interfaces are important in a wide range of technologies. The interfacial morphology can determine the performance characteristics of dissimilar material joints, metal–matrix composites, ceramic–matrix composites, electronic packages, glass-to-metal seals, glass processing systems, and liquid–metal processing systems. Microstructural development on ceramic–metal interfaces plays a critical role in all of these processes[7].

In the literature, there are only a few papers which describe the diffusion phenomena in the friction welding process and most involve similar and dissimilar metals.

*e-mail: zainal@eng.usm.my

Taban et al.[8] studied the friction welding of 6061-T6 aluminum and AISI 1018 steel and suggested that a thin, discontinuous intermetallic layer formed at the bondline was a result of interdiffusion between iron and aluminum. Intermetallics generally result in mechanical degradation of the joint. The formation of these phases is mainly driven by interdiffusion of the species and is highly dependent on the specific time and temperature history of the welding process. The extended thermal cycles (higher temperatures/longer times) associated with fusion welding processes generally result in the formation of thick intermetallic compound (IMC) layers at the joint interface. The formation of these layers is generally considered the root cause for property degradation seen with these types of joints. FW can facilitate joint formation at lower temperatures, often at very short times, and is generally associated with reduced formation of these intermetallic phases[9,10]. For ceramics–metal welding, the intermediate layer apart from thermo-plastic deformations of metal plays a significant role. It seems that besides adhesion, the diffusion of atoms from the metal layer into the ceramic foundation can cause sealing of a ceramic material with metal. This is confirmed by the results of investigation on linear distribution of elements, carried out by means of electron probe techniques. The gradient of aluminum concentration, temperature gradient and stress field are the factors that power the atom migration in metal during the welding process. Zimmerman et al.[11] predicted the average diffusion coefficient of Al to Alumina ($D = 1.8 \times 10^{-13}$ m^2/s) in friction welded Alumina-Al6061 and stated that the diffusion region occurred in several micrometers distances.

The purpose of this paper is to analyze mechanical strengths and interfacial properties in bonded alumina-mild steel rods during the friction welding process where an interlayer Al6061 sheet is used. A preliminary simulation is made to predict the deformation, stress, strain and temperature distribution during the joining operation using a fully coupled thermo-mechanical FE model.

2. Experimental Methods

2.1. *Material and sample preparation*

In the experimental study, rods 10 mm in diameter made of alumina (50 mm length) and mild steel (50 mm length), and Al6061 sheet (0.3 mm, 0.5 mm, 1.0 mm and 1.5 mm) interlayers were used. The connection surfaces of mild steel and alumina were ground to smooth and sharp edges around it. The experimental setup for the FW process is shown in Figure 1.

The friction welded sample was sectioned perpendicular to the weld interface and polished. Macrograph and microstructure of the weld interface were obtained using Dino-Lite digital microscope and Field Emission Scanning Electron Microscopy (FESEM) (model VPFESEM SUPRA 35VP) machine repectively. Electron-probe microanalysis (EPMA) was carried out across intermediate layers to determine the variation of element concentration using FESEM. The successfully welded samples at various friction times were also measured for their four point bending strength using Instron machine (model 8501) and Knoop hardness test.

The friction welding process was done on a continuous drive friction welding machine. The friction welding conditions were 900 rpm rotational speed and 20 MPa axial pressure. The bending strengths and hardness values of the welded samples were determined. The successful joined alumina-mild steel rods are shown in Figure 2.

2.2. *Mathematical model of FW*

2.2.1. Heat transfer

The governing energy balance for heat flow with a moving heat source in an elementary volume subjected to thermal straining may be expressed as:

$$pc\dot{T} + div\left[-k'.grad(T)\right] = \dot{Q} \quad (1)$$

where $T(x,y,z,t)$ is temperature, (x, y, z) are coordinates in the domain D, $\rho = \rho(T)$ is the density, $c = c(T)$ is mass specific heat, $k' = k'(T)$ is heat conductivity and $\dot{Q}$ (x,y,z,t) is volumetric heat generation.

The main heat source in FW is generally considered to be the friction between the rotating rod (mild steel)-interlayer (aluminum alloy) sheet surfaces and the unrotating rod (alumina)-interlayer (aluminum alloy) sheet surfaces, and the "cold work" in the plastic deformation of the interlayer. The heat generation from the plastic deformation of the aluminum is considered to some extent in the model with the use of variable friction coefficient and not explicitly accounted for as a heat source. The heat is generated at the interface of the rotating steel rod and the aluminum sheet due

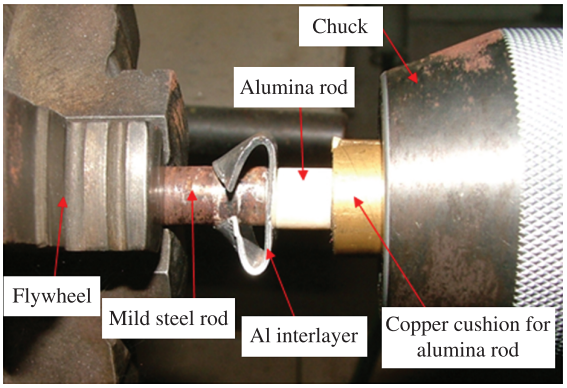

Figure 1. Experimental setup for the FW process.

Figure 2. Successful joined alumina-mild steel rods.

to friction and plastic deformation. Frictional heat generated at the contact surfaces of steel-aluminum (85-90% of total heat) is analytically determined as follows[11]

$$q_1 = \mu P \omega r \tag{2}$$

Heat due to plastic deformation (10-15% of total heat):

$$q_2 = \eta \sigma \dot{\varepsilon}^{pl} V \tag{3}$$

where η is the inelastic heat fraction, which is assumed to be constant, σ is the stress, $\dot{\varepsilon}^{pl}$ is the rate of plastic straining, and V is material volume.

Heat into mild steel and alumina rods from interfaces of mild steel-aluminum and alumina-aluminum:

Heat into mild steel, $q_s = 0.5(q_1 + q_2)$ (4)

Heat into alumina $q_a = 0.5(q_1 + q_2)$ (5)

The heat generated at the surface of the steel is transferred into the steel itself following the Fourier's law of heat conduction. The heat transfer equation for the steel rod in a static coordinate system is

$$pc\frac{\partial T}{\partial t} = \dot{Q} + k'\left[\frac{\partial^2 T}{\partial x^2} + \frac{\partial^2 T}{\partial y^2} + \frac{\partial^2 T}{\partial z^2}\right] \tag{6}$$

where T is the temperature, c is heat capacity, ρ is the density and k' is heat conductivities that vary with temperature in the calculations. The aluminum workpiece is considered to have isotropic material property and same value of thermal conductivity is used for all three directions.

The coordinate system moves over the workpiece in the positive x-axis at a velocity u_x. The heat transfer equation for the workpiece is:

$$pc\left(\frac{\partial T}{\partial t} + u_x\frac{\partial T}{\partial x}\right) = \dot{Q} + k'\left[\frac{\partial^2 T}{\partial x^2} + \frac{\partial^2 T}{\partial y^2} + \frac{\partial^2 T}{\partial z^2}\right] \tag{7}$$

2.2.2. Boundary and initial conditions

The conduction and convection coefficients on various surfaces play an important role in the determination of the thermal history of the workpiece in friction welding. The initial and boundary conditions considered in this model are based on the actual conditions exhibited in experiment. Figure 3 shows the various boundary conditions applied on the model.

Convection at the sides of the aluminum alloy sheet and the rods is represented based on Newton's law of cooling as

$$k'\frac{\partial T}{\partial n_o}\Big|_\Gamma = h\left(T - T_{amb}\right) \tag{8}$$

where n_o is the normal direction vector of boundary Γ and h is the convection coefficient. The convection coefficient is h_s at the side of the steel rod, h_{al} at the sides of free surface of aluminum alloy sheet, ha at the side of the alumina rod exposed to ambient.

In addition, the initial condition must be specified for (x, y, z)$\in$ D:

$$T(x, y, z, 0) = T_o(x, y, z) = T_{amb} \tag{9}$$

If the partial differential Equation 7, the boundary condition 8, and initial condition 9 are consistent the problem is well posed and a unique solution exists. Frigaard et al.[12] states that during the welding period, heat generation equations can be directly used in the model development as long as the contribution from plastic deformation and the variable frictional conditions at the rod/interlayer sheet interface are accounted for by the reasonable average value for friction coefficient. In the case of aluminum alloys, the local melting will occur if the material is heated above its solidus temperature. But from the temperatures obtained in the aluminum workpiece from previous work, it is generally understood that the workpiece never reaches its solidus temperature. The friction coefficient is assumed to change between 0.4 and 0.5. Frigaard et al.[12] use the coefficient of friction value as 0.5 for the condition of sticky friction and 0.4 for the condition of partial sliding and sticky friction. The friction coefficient is considered to decrease from 0.5 to 0.4 as the temperature increases at the interface of rod and workpiece.

2.2.3. Thermo-mechanical model

The thermal model was sequentially coupled to the mechanical model. The workpiece was constrained in movement based on actual experimental setup. The mechanical loading of unrotating rod was considered retaining the load step size used in the thermal model. The

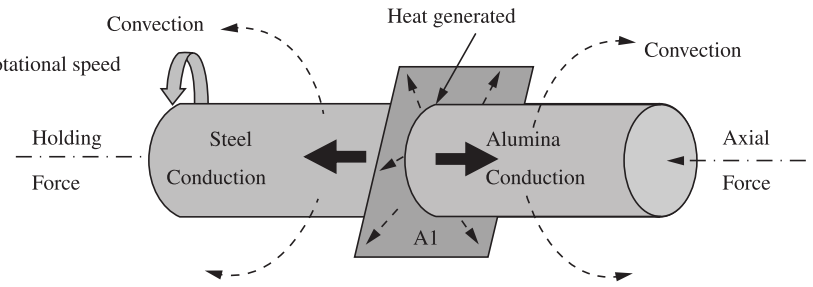

Figure 3. Boundary conditions applied on steel rod, alumina rod and aluminum alloy sheet.

temperature history of the rod was considered in each load step with the mechanical loading to calculate the active stress developed in the workpieces. The quasi-static motion of an elementary volume is governed by the rate form of equilibrium between stress and body forces is

$$div\dot{\sigma} + \dot{p}_v = \rho a \tag{10}$$

where $\dot{\sigma}$ is the stress tensor, $\dot{p}_v$ is the volume force intensity, ρ is the material density and a is the acceleration. The inertial effect is neglected (*a* is neglected) in the model since a constant rotational speed and welding speed is used during FW.

The mechanical rate and history effects are affected by the extreme range of temperatures, the high temperature gradients and the large variation of temperature rates. The mechanical response behavior is decomposed into thermal, elastic and plastic components.

The total strain $d\varepsilon'_{ij}$ is composed of elastic strain $d\varepsilon'_{eij}$, plastic strain $d\varepsilon'_{pij}$, and thermal strain $d\varepsilon'_{Tij}$:

$$d\varepsilon'_{ij} = d\varepsilon'_{eij} + d\varepsilon'_{pij} + d\varepsilon'_{Tij} \qquad (i,j= 1,2,3) \tag{11}$$

Hooke's law, written in subdivided form according to deviatoric and dilatoric or volumetric portion, applies to elastic strain:

$$\varepsilon'_{dij} = \frac{1}{2G}\sigma_{dij} \tag{12}$$

$$\varepsilon'_{vij} = \frac{1}{3K}\sigma_{vij} \tag{13}$$

The tangent modulus *G* and compression modulus *K* can be expressed by the elastic modulus *E* and Poisson's ratio *v*':

$$G = \frac{E}{2(1-v')} \tag{14}$$

$$K = \frac{E}{3(1-2v')} \tag{15}$$

The thermal strain ε'_T is given by dilatoric strain components which are function of thermal expansion coefficient:

$$d\varepsilon'_{Tij} = 3d\varepsilon'_T = 3\alpha_T dT \tag{16}$$

where α_T is the thermal expansion coefficient, *E* is elastic modulus, *v*' is the

Poisson's ratio, and σ_Y is the yield strength.

2.2.4. FEM model

To model the actual physics phenomena of the FW process is rather complicated. Therefore, several simplifying assumptions have been made. The assumptions made when defining the loads and boundary conditions for the simulation are

- Perfect elastic-plastic behaviour of the work pieces material was assumed also to reduce computer time requirements;
- The interlayer and rods were assumed to experience frictional contact described by Coulomb's frictional law with temperature dependent friction coefficient, μ;
- The friction coefficient, μ below material melting point were assumed to be zero following the tendency from the experimental chart[13];
- The radiation heat loss was neglected as it was considerably less compared to the conduction and convection losses. The finite element thermo-mechanical model used the temperature varying material properties (thermal conductivity, specific heat and density) for the rods and interlayer. There was assumed to be no material melting since the maximum temperature was maintained below the solidus temperature (582 °C) of the aluminum alloy;
- Almost 90% of the nonrecoverable work because of plasticity was assumed to heat the work pieces. This was the fraction of inelastic dissipation rate that appears as a heat flux per unit volume; and
- 100% of dissipated energy caused by friction between parts was converted to heat and distributed evenly between the two interacting surfaces.

The alumina and steel rods were modelled in the computational domain of 20 mm length and 10 mm diameter each. The aluminum alloy sheet was modeled in the computational domain of 1.42 mm thickness and 12 mm diameter. The alumina and steel rods were modelled using 3D solid (continuum) elements as deformable rigid constrained bodies by Abaqus 6.8 software package. The aluminum sheet was modelled as a solid and deformable element. The attachment of aluminum sheet to the steel rod end surfaces was considered to be perfectly tied.

In this analysis, a uniform connection was assumed. The plasticized zone was the heat generated and affected area where the aluminum turned to be softened due to severe friction. In this zone the material model of Johnson-Cook and adaptive meshing were incorporated during simulation to enable the occurrence of the aluminum deformation. Coulomb friction law has been selected for the modelling of the workpieces interface contact. Heat transfer is allowed on the components contact area. The boundary conditions, contact conductance in the heat sink, the convection on the external surfaces and sliding surfaces on contact surfaces are applied on the assembled components of aluminum, steel and alumina. Initial temperatures for all components were assumed at 29 °C. The aluminum alloy edge was constrained to move axially.

Since the FW process involves large deformation, adaptive meshing minimizes element distortion when an Arbitrary Lagrangian-Eulerian (ALE) approach is used in comparison with a solution using the Lagrangian approach with an implicit solver. Also, the contact algorithm used by Abaqus/Explicit is computationally efficient when compared to an implicit solver.

The three components were modelled as 3D solid linear thermally coupled brick using linear hexahedron element having eights nodes with three degrees of freedom with tri-linear displacement, temperature calculation and hourglass control. They have been meshed using element type C3D8RT, which has 8-node tri-linear displacement and temperature and reduced integration with hourglass control. A total of 3963 elements and 5534 nodes have been generated in Abaqus 6.8 explicit nomenclature as shown in Figure 4. Their size varies from 0.4 mm to 2 mm depending on the parts.

In order to reduce processing time and to simplify the model, the two rods were modelled and constrained as 3D discrete rigid parts. Rigid elements can be used to define the surfaces of rigid bodies for contact and can be used to define rigid bodies for multibody dynamic simulations. The holding chucks at the end of the two rods were not modeled in the simulation. Instead, the thermal and mechanical interactions between the contact surfaces were represented by the application of appropriate distributed heat fluxes in the heat transfer analysis and by the application of appropriate concentrated loads in the steady-state transport analysis, respectively.

The FE analysis was conducted by prescribing steel rod rotation and followed by displacement of the alumina rod with appropriate boundary conditions. The friction welding simulation was prescribed in three time steps, based on an actual experimental setup. In the first step, the steel rod was rotated at angular velocity of 94.3 rad/s. Then in the second step, the alumina rod was axially displaced with a rate of 20.8 m/s to the aluminum alloy sheet. Lastly in the third step, after the rubbed interface reached appropriate welding temperature, the rotating steel rod was stopped for cooling stage.

In this example the dissipation of the frictional heat-generated temperature fluctuates, ranging from a minimum value of 40 °C to a maximum value of 560 °C over the entire friction welding cycle. The temperature

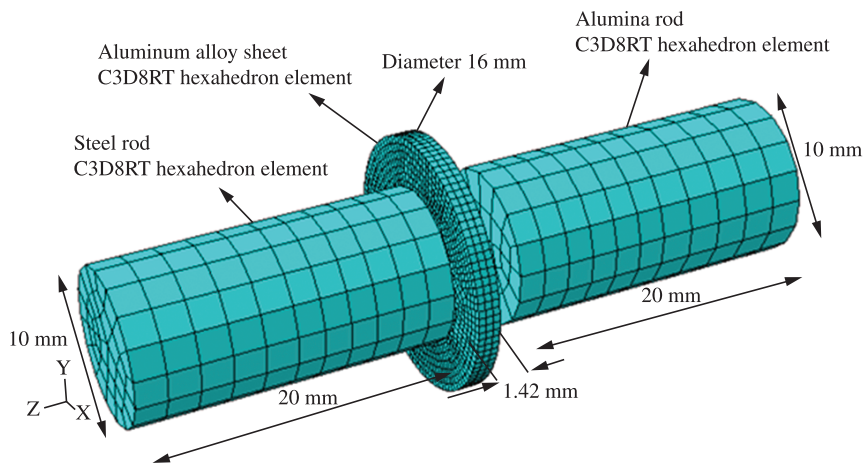

Figure 4. The FEM model and dimension of the workpieces assembly of friction welding process in Abaqus 6.8.

Table 1. Material properties of aluminum alloy 6061-T6, alumina and steel.

Material	Temperature (°C)	Thermal conductivity ($W.m^{-1}.K^{-1}$)	Heat capacity ($J.kg^{-1}.K^{-1}$)	Density ($kg.m^{-3}$)	Thermal expansion ($\times 10^{-6}\ K^{-1}$)	Young's modulus (GPa)	Yield stress (MPa)	Poisson's Ratio	Melting point (°C)
Aluminum alloy 6061-T6	0	162	917	2703	22.4	69.7	277.7	0.33	582-652
	98	177	978	2685	24.61	66.2	264.6		
	201	192	1028	2657	26.6	59.2	218.6		
	316	207	1078	2630	27.6	47.78	66.2		
	428	223	1133	2602	29.6	31.72	17.9		
	571	253	1230	2574	34.2	0	0		
Alumina	25-727	16.7	950	3950	7.5	300	-	0.2	2127
Steel	0	34.5	470	7800	10.1-16.6	68.9-207	-	0.23-0.3	1230-1530
	98	345	485						
	201	33.8	520						
	316	31	560						
	428	28.5	620						
	571	26.8	700						
	650	25.8	760						

distribution when the contact surfaces are heated to its peak value. Under such operating conditions plastic deformation, as well as creep deformation, is observed. The Johnson-Cook plasticity model, which was best suited for modeling the response of materials with significant time-dependent behavior as well as plasticity at elevated temperatures, was used to model the aluminum behaviour. This material model consists of an elastic-plastic network. Because the elastic-plastic response of the material varied greatly over this temperature range, temperature-dependent material properties from Table 1 were specified. Table 2 shows the input parameters for the friction welding process simulation.

3. Results and Discussion

3.1. *Mechanical properties*

3.1.1. Bending strength

The reliability of friction-welded ceramic-metal joint with the use of interlayer depends upon the bending strength of the joint which is usually related to interlayer thickness and friction time of the joint. In this section, the relationships between the interlayer thickness, friction time and bending strength were investigated. Here, the bending strength was

Table 2. Friction welding condition for the process simulation.

Condition	Parameter/symbol	Value
Material model for Aluminium Alloy		
AA6061-T6:	*A* [MPa]	324
Plasticity	*B* [MPa]	114
Johnson-Cook Law	*n*	0.42
	m	1.34
	melting point, °C	582
Rate Dependent:	C	0.0083
	Epsilon dot zero	1
ALE Adaptive mesh domain:	Frequency	10
	Remeshing sweep per increment	3
ALE Adaptive mesh control:		
	Initial feature angle	30
	Transition feature angle	30
ALE Adaptive mesh constraint:	Mesh constraint angle	80
Inelastic heat fraction	(β)	0.9
Contact:		
Thermal conductance :	(K_i) [$W.m^{-2}.K^{-1}$]	1.108
Heat Partition coefficient :	(Γ)	0.5
Friction coefficient temperature dependent:	(μ)	0.28 (0 °C)
	(i) Alumina/aluminum contact[11]	0.32 (93 °C)
		0.34 (201 °C)
		0.38 (316 °C)
		0.42 (428 °C)
		0.26 (571 °C)
		0.16 (650 °C)
	(i) Steel/aluminium contact[14]	0.61 (22 °C)
		0.545 (34.7 °C)
		0.259 (93.3 °C)
		0.115 (147.5 °C)
		0.064 (210.6 °C)
		0.047 (260 °C)
		0.035 (315.6 °C)
		0.020 (371.1 °C)
		0.007 (426.7 °C)
		0(582 °C) (melting point)
	(η)	
Friction energy transformed into heat :	penalty	0.9
Interaction mechanical constraint formulation :		
Process:		
Displacement (depth of plunge)	(m)	0.0009 (0.9 mm)
Axial Pressure	(MPa)	9.5
Rotational Speed	rad/s	94.3 (900RPM)
Initial temperature	°C	29

the average value of 4 joints welded under the same welding conditions. Most of the tested samples fractured in the alumina rod part indicating that the joint is stronger than the brittle alumina body. Most of the tested samples fractured in the alumina rod part as shown in Figure 5. This indicates that the joint is stronger than the brittle alumina body.

Figure 6 shows the graphed relationship between the interlayer thickness, friction time and bending strength of the joints. The use of interlayers 1.0 mm and 1.5 mm in thickness revealed that the bending strength increased almost proportionally with the increase in friction time ranging from 60 to 200 MPa, except for joints with 0.3 mm and 0.5 mm interlayers.

The joints with 1.0 mm and 1.5 mm interlayer exhibit the maximum bending strengths at the friction time of 20 seconds i.e. 191 MPa and 186 MPa, respectively, while the bonds with thinner interlayers (0.3 mm and 0.5 mm) show lower bending strength values between 40 to 150 MPa. The thinner interlayers could not maintain the increment of the strength after 8 seconds and 18 seconds because they have been largely depleted, leaving an insufficient amount of interlayer for joining. Actually, some of the hot deformed interlayer is expelled out from the interface area during friction welding. The remaining pressed plasticized interlayer diffuses to the alumina and the mild steel surfaces to produce bonds between them. The insufficient remaining interlayer will incur the existence of incomplete joint near the periphery of the interface which is detrimental to the joint strength. Figure 7 shows the strong bond at the middle part of the joint.

Apart from that, the incomplete joint could also exist due to major differences in melting points and higher surface energy[15]. Thus, it usually exists at the alumina-aluminum interface rather than at the mild steel-aluminum interface because alumina has a higher melting point.

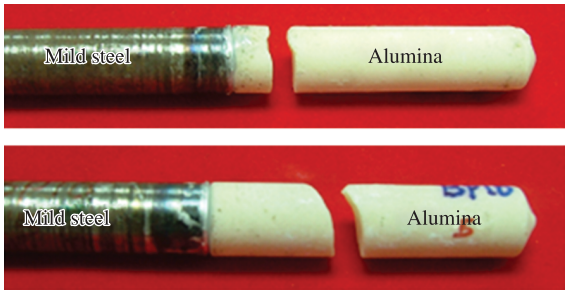

Figure 5. Fractured alumina rods after bending tests.

3.1.2. Hardness property at different point near the bondline

The hardness profile near the bondline of the alumina-mild steel joint is shown in Figure 8. The hardness profile in the alumina part exhibited insignificant change and remained constant like before the friction process occurs, i.e. within the range of 1300-1700 KHN. Because alumina has inert, hard and brittle properties, only aluminum atom diffusion occurs at the contact surface during the friction process. On the other hand, the hardness value for the mild steel part slightly increased towards the joint (reaching 200 KHN). This resulted from the effects of the formation of the narrow brittle intermetallic phase at the mild steel–aluminum interface, as discussed in the interfacial microstructure characterization.

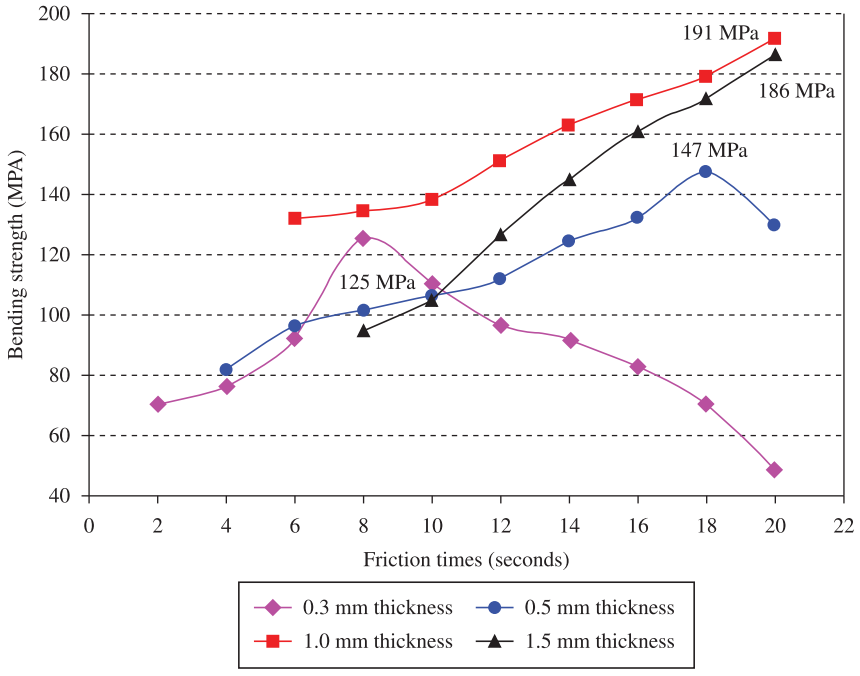

Figure 6. Relationship between interlayer thickness, friction time and bending strength of the joints.

3.2. *Interfacial properties analysis*

The interfaces of the welded sample were observed and analysed. The weld cross-section of successful mild steel and alumina rods joint with the use of Al6061 interlayer is shown in Figure 9. The two rods were bonded by the interlayer with an average intermediate distance of 0.303 mm. The friction process had consumed about 0.997 mm of the original interlayer thickness (1.3 mm) to create the joint.

3.2.1. Aluminum diffusion across aluminum-alumina interface

Aluminum elements across the aluminum-alumina interface are presented in Figure 10. The interfacial microstructure of the aluminum-alumina interface with visible bond seam can be obviously seen in Figure 10a. The alumina-aluminum interface does not show the presence of any new phase except for mechanical interlocking of alumina and aluminum.

Alumina is a very stable ceramic and it only allows reactions to occur at higher sintering temperatures (1600 °C). Alumina surface is porous, inert, rigid and has an open structure, as shown in Figure 10a. The bonding occurs at the interface by mechanical mixing and interlocking mechanism whenever plasticized aluminum atom diffuses into the alumina surfaces. Mechanical mixing and interlocking occurs at the alumina-aluminum interface.

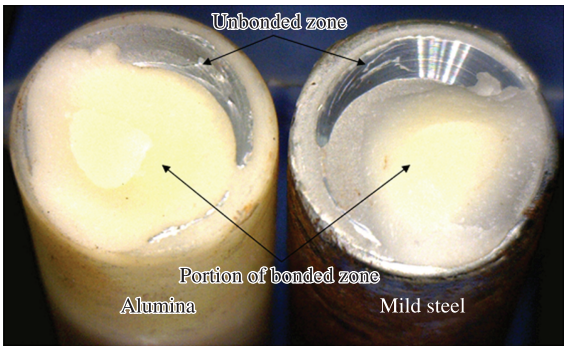

Figure 7. Macrograph of the tested sample fractured at the interface.

Al concentration varies from the aluminium side (97.92 wt. (%)) across the interface towards the alumina side (78.19 wt. (%)). During the friction welding process, the softened Al is expected to diffuse into the alumina side in micrometer distance, causing interlocking and mechanical mixing with the open structure of the alumina surface for interface bond formation.

3.2.2. Aluminum diffusion across aluminum-mild steel interface

The friction process of dissimilar metals can produce an intermetallic region at the interface area[16]. Figure 11a shows the enlarged interfacial microstructure of mild steel-aluminum with the presence of a very narrow intermetallic compound, which seems to be caused by extreme rubbing action and reaction in the contact zone. The intermetallic phase was clearly detected by EDX analyzer (Figure 11b) as a combination and variation of elements of Al and Fe. This compound is brittle and could be detrimental to the joint strength if its formation is not controlled. A longer duration of the friction process could produce more intermetallic compound[10]. Therefore, controlling the friction time limits the growth of the intermetallic phase at the mild steel-aluminum interface. Usually, a very short friction time is attempted to avoid wider intermetallic phase formation.

The results in Figure 11b show linear traces of Fe and Al contents in wt. (%). Based on the Fe-Al phase diagram[17], the intermetallic compounds are identified with their corresponding crystal structure in Table 3. Based on the compositions from Table 3 and Figure 9b, the Fe-rich intermetallics (FeAl and Fe_3Al) and the Al-rich intermetallics ($FeAl_3$ and Fe_2Al_5) can be identified. It should be noted that the $FeAl_3$ and Fe_2Al_5 intermetallics are brittle while FeAl and Fe_3Al are slightly ductile[17]. A relatively smaller number of steel fragments are present at the aluminum side.

3.3. *Analysis of 3D FE model of FW*

The interlayer is compressed to maximum extent initially only due to the mechanically induced strain and the corresponding force in axial position is recorded as the maximum force. When a thermo-mechanical steady-state is

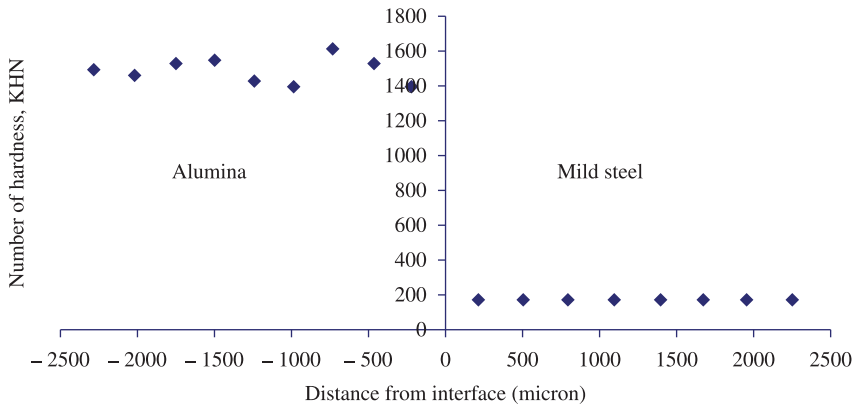

Figure 8. Result of microhardness test of alumina–mild steel joint.

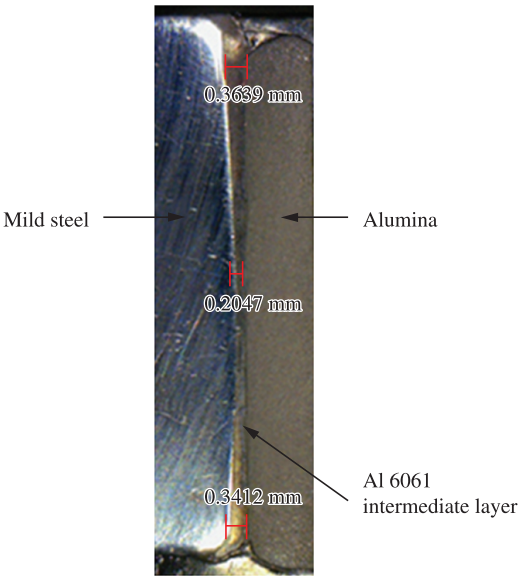

Figure 9. Digital micrograph of the weld cross-section of the joint with 0.303 mm average Al6061 intermediate layer thickness.

Table 3. Compositions and crystal structures of intermetallic compounds of Fe-Al.

Type of intermetallic compound	wt. (%) of Fe	Crystal structure
Fe_3Al	86.06	FCC
FeAl	67.31	Cubic
$FeAl_2$	50.72	Triclinic
Fe_2Al_5	45.16	Monoclinic
$FeAl_3$	40.70	Monoclinic

attained by the workpiece, flash of the joint is formed at the interfaces as clearly seen in Figure 12. It is observed that the flash increases at the periphery of the alumina rod due to the deeper plunge of the rod displacing more material from the TMAZ in the aluminum sheet.

3.3.1. Deformation of the interlayer

The thermo-mechanical state of the workpiece during the process leads to the softening of matrix in the interlayer, and also leads to the unloading of the machine and in turn reduction in the plunge force as observed in the temperature variation during friction welding simulation process. Figure 13 shows simulation of the deformation of the interlayer for time running period of 0.01 seconds and the rod rotation speed of 900 rpm. The value of maximum rod displacement occurring at the interface contact is about 0.9 mm. The maximum displacement of material occurs radially from the compressed area to the uncompressed zone near the periphery of the joined rods.

The rod plunge starts to increase as the temperature builds up in the workpiece. The deformed shape does not resembles that experimentally observed, shown in Figure 12 because the coarse mesh was used to save the Abaqus running period. The flash from the interlayer could be obtained if more refiner mesh size is used for the interlayer. In this study the approach of using Abaqus software is just for preliminary study where the visualization of the whole FW dynamic process could be carried out with few analyses.

3.3.2. Temperature distribution

Since the heat flux is generated at the rod/interlayer interfaces, the heat flows through the intermediate layer into the alumina and steel rods creating a thermal profile.

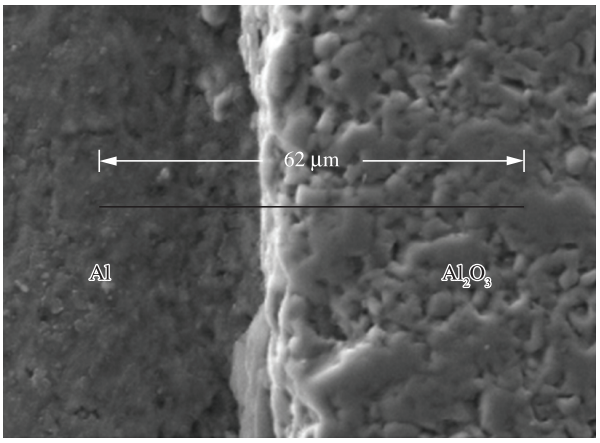

(a)

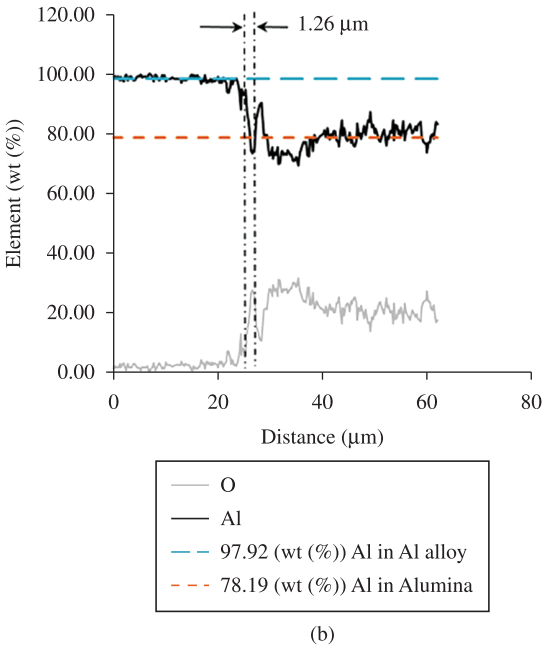

(b)

Figure 10. a) The 62 µm length tested zone across the aluminum-alumina interface. b) Linear distribution of the chemical elements performed by EDX analysis across the interface.

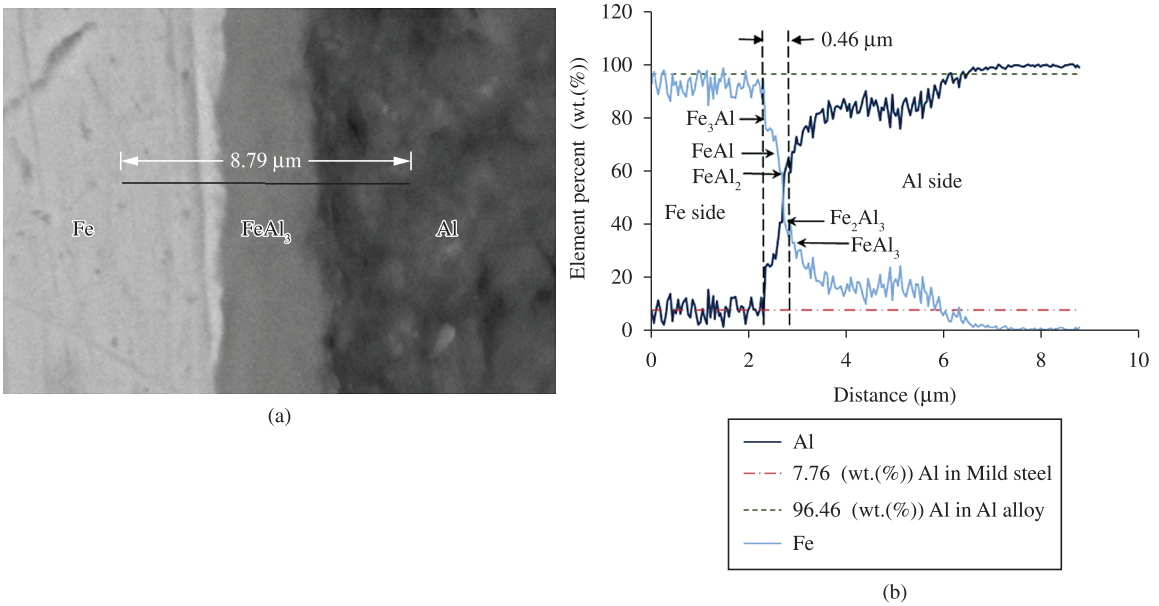

Figure 11. a) The 8.79 µm length tested zone across the aluminum-mild steel interface. b) Linear distribution of the chemical elements performed by electron probe X-ray microanalysis across the interface.

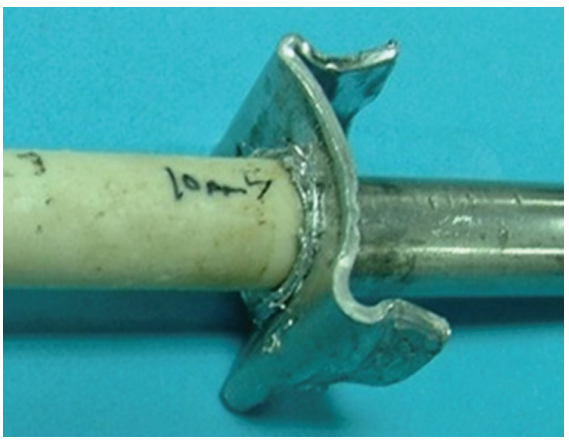

Figure 12. Appearance of friction welded alumina-mild steel with aluminum alloy interlayer.

The simulation is stopped when the maximum aluminum temperature reached reasonable value below its melting point as discussed earlier in section 5.3.1 and reported in many FW based literature involving aluminum alloy[18,19]. It is observed that the heating temperature of the aluminum-alumina is in the range of 400-450 °C to obtain the joint as has been claimed in the past from other author[11]. Table 4 shows the variation of the temperature in the cross-section of the joint and the rubbing surface of the interlayer throughout the simulation run for the constant steel rod rotation speed of 900 rpm. Increase rapidly in axial load increases the surface heat flux in the deformed aluminum, particularly in the region adjacent to the rods periphery. This leads to higher temperatures which are observed in the simulation results. As it can be observed a maximum temperature of 449.4 °C has been achieved in the early deformed aluminum sheet at 0.0001 seconds. The maximum rubbing temperature is also almost correlative with the predicted output finite difference thermal model as developed by Seli et al.[20]. As the friction persists, the maximum temperature drops to 224.1 °C at 0.01 seconds and decreases further down to 177.1 °C after 0.01 seconds the rod rotation the is stopped. The previous papers[21] have described the phenomena of drop in friction coefficient at temperatures close to melting point leading to a drop in heat flux value on the interfaces. This change has been considered during the modeling effort in the scope of this research. While preparing the model, it was found that including the effect of the elastic slip between the aluminum sheet and the alumina rod surfaces is crucial to obtain reasonable results for the temperature distribution.

As can be seen in the last column in Table 4, the highest temperatures occurred in the material close to the rod periphery, and the temperature rapidly and non-uniformly decreased as the distance far from the periphery. Some parts at the center rubbing surface seem to have higher temperature compared to the middle region between the periphery and center regions. The shape of the temperature contours seems to be reasonable fashion the shape of the heat affected zone corresponding to the consideration of the combination of the rotation and axial loading. When the rod rotation is stop at 0.02 seconds, the cooling rubbed surface shows uniform temperature distribution. Good bonding is expected to occur at the region near periphery of the rod rubbing surface corresponding to the higher temperature distribution and deformation observed on the region.

In the numerical simulation the flux value in individual nodes on the contact surface was dependent on the changing friction coefficient with temperature. Figure 14 shows

time-temperature history of nodes 55, 239 and 245 on the alumina rubbing surface as labeled in the inset. The wavy like temperature increase on the nodes most probably due to the friction and the interlayer surface deformation. Node 55 has a steady temperature increase from room temperature up to 100 °C over as it located at the periphery of the rod. Node 245 at the center of the rod indicates up to around 78 °C higher temperature that of middle node 239. These temperature variation correlates with the temperature contours of the interlayer rubbing surface discussed above. After the rod rotation is stopped, the three nodes maintain receiving constant heat flows from the higher temperature deformed aluminum sheet.

Unlike alumina, it is expected that steel has much higher temperature increase as illustrated in Figure 15. The comparison thermal conductivity between steel and alumina has been discussed in detail by Seli et al.[20]. As labeled in the inset in the Figure 15, node 56 located at the rod periphery has the highest temperature increase. The temperature increase rapidly from room temperature up to almost 130 °C. Due to friction mechanism, the temperature then rises and fluctuates further until 150 °C before slowly decreases when the steel rod rotation is stopped. Following the same trend, both inner nodes 245 and 250 show overlap curves. During the FW process, temperature at the two nodes increase rapidly up to 110 °C and steadily rises up to 150 °C before slowly decreases after the FW stopped.

3.3.3. Strain and stress distribution

Figure 16 shows the Von Mises stress and equivalent plastic strain contour maps of the interlayer rubbing surface at friction welding time of 0.0053 seconds. As it can be observed, the maximum plastic strain reaches the value of 6, and is generated where the largest plastic strains take

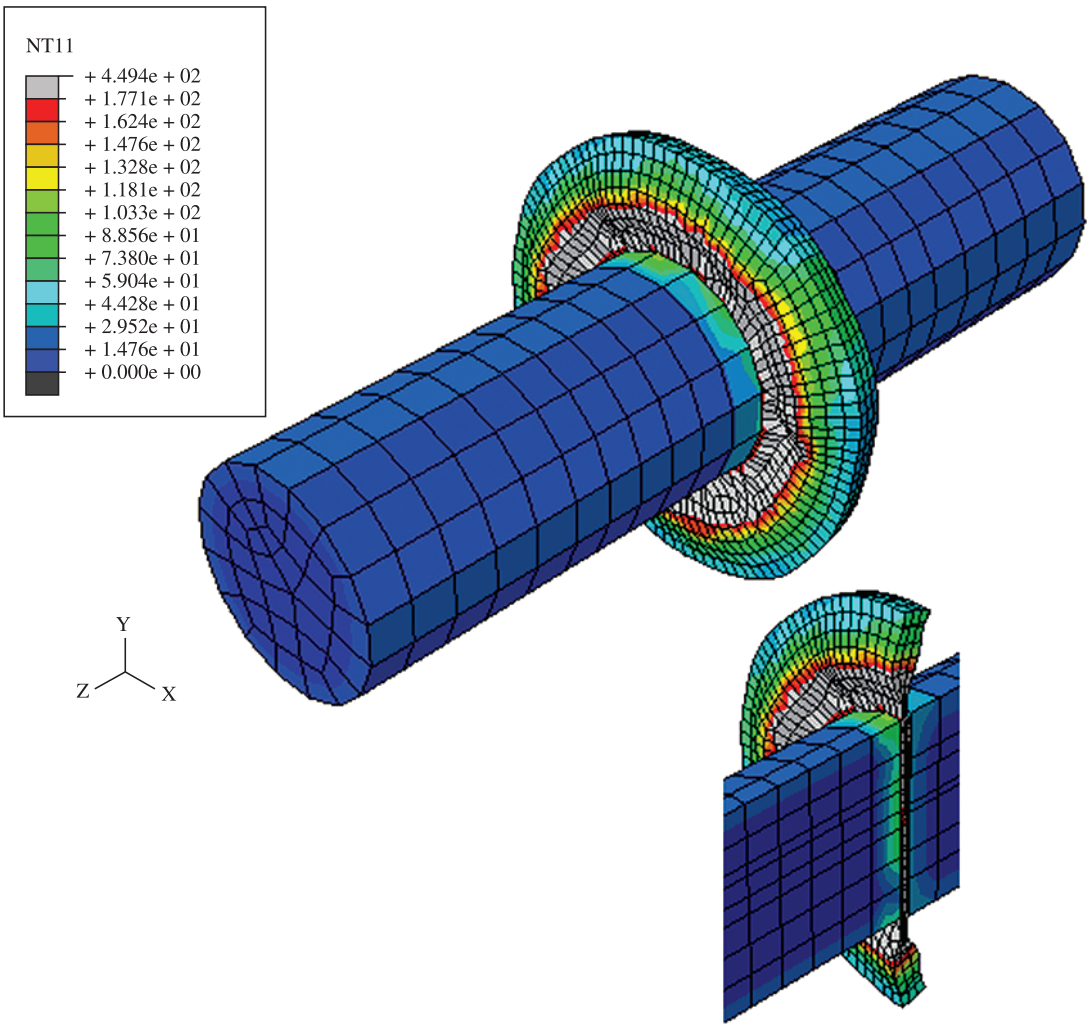

Figure 13. Top: Total deformation of the interlayer due to the horizontal displacement under mechanical loading and rotation (900 rpm). Bottom: Cross section view of the interlayer deformation across Eulerian boundary.

Table 4. Series of temperature changes for the FE model of the 3D FW.

Total time	Cross section view	Interlayer rubbing surface view
0 seconds (initial)	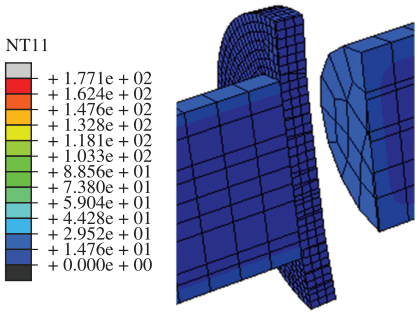	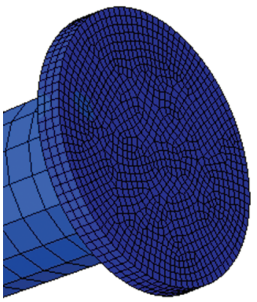
0.0001 seconds	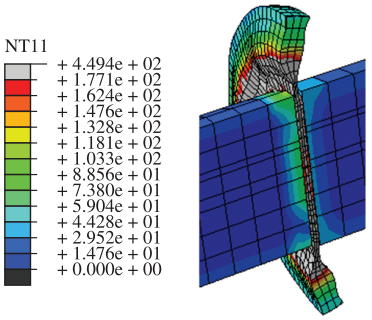	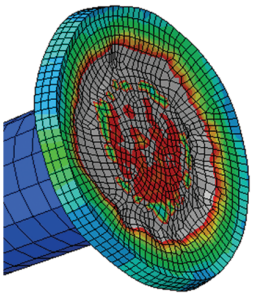
0.005 seconds	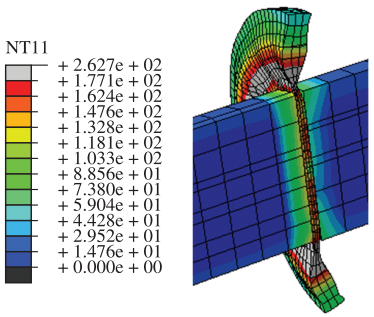	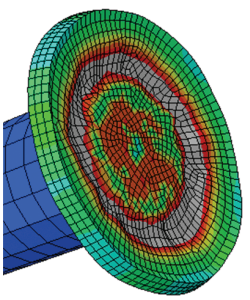
0.01 seconds	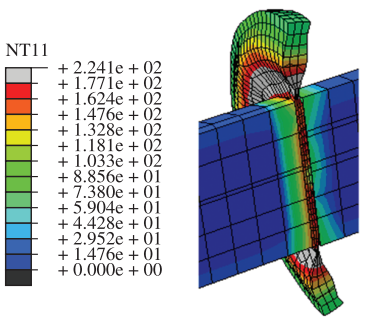	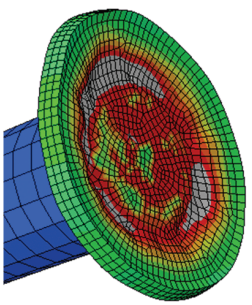
0.02 seconds (0.01 seconds after rotation stopped)	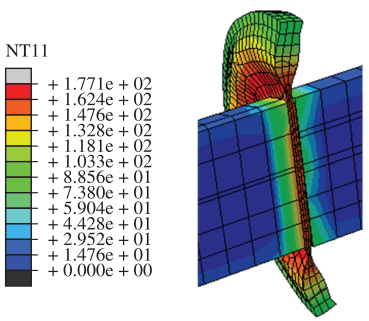	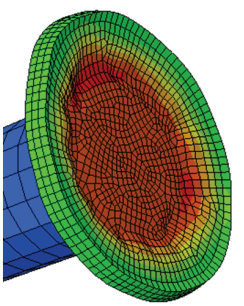

place in the material close to the rod periphery, since the material is subjected to intense deformations due to the rod's translational and rotational motion. This issue matches with the maximum deformed interlayer temperature found at the same zone.

Regarding the Von Mises stress distribution shown in Figure 16, it is important to keep in mind that, in the model, the yield stress was given as a function of temperature and the values ranged from around 510 MPa at room temperature to less than 21 MPa at temperatures greater than 300 °C. As can be observed, The material close to the contacted rod experienced yielding and the maximum stress appears in the interlayer contacted surface, near the periphery zone of the contacted diameter.

There are several key parameters in the model that have a significant impact in the simulation results: the coefficient of friction between the rod and the interlayer material, the limiting shear stress that controls the stick/slip condition between contacting surfaces and the distribution of frictional heat between the rod and the interlayer sheet. Ideally, carefully designed experiments should be conducted to determine the value of those parameters.

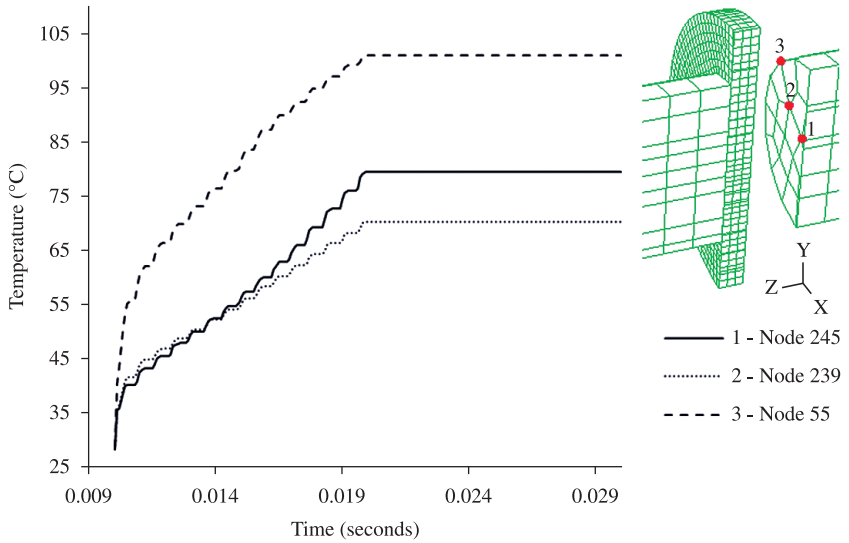

Figure 14. Temperature at nodes 55, 239 and 245 on the alumina rubbing surface as a function of time during the entire process period.

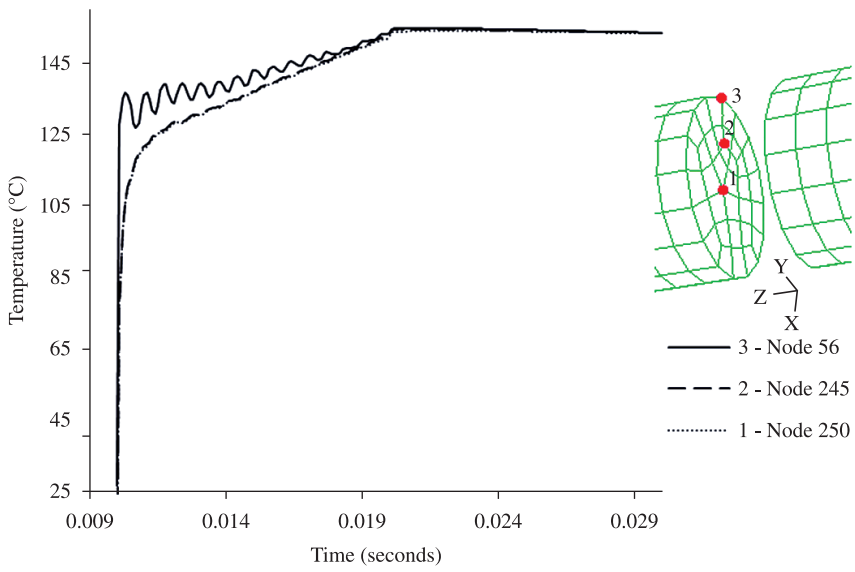

Figure 15. Temperature at nodes 56, 245 and 250 on the tied steel-aluminum interface as a function of time during the entire process period.

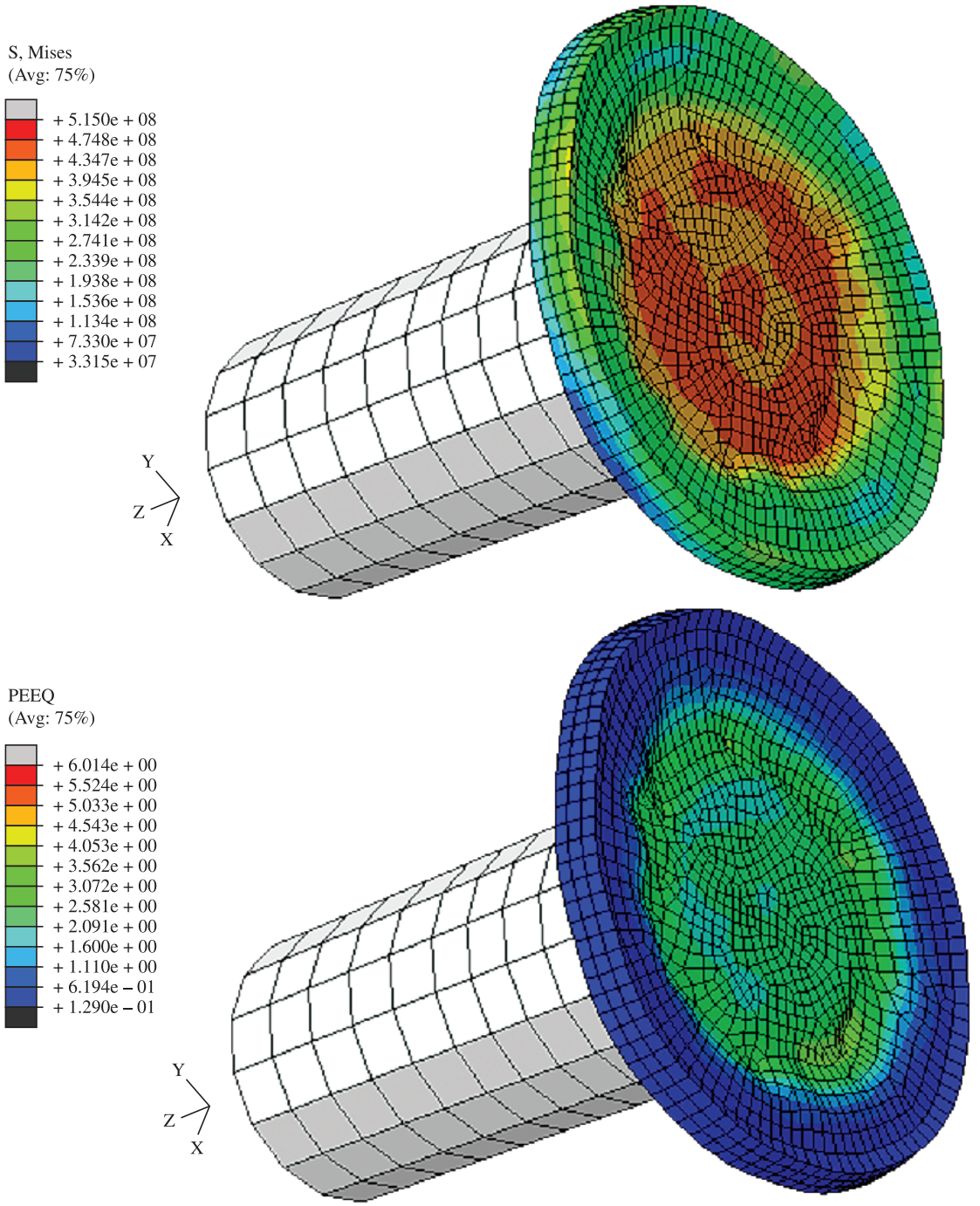

Figure 16. Von Mises stress (top) and equivalent plastic strain (bottom) for the interlayer rubbing surface.

4. Conclusions

This work demonstrated the creation of bond through interfacial interlocking and intermetalllic phase formation with average joint bending strengths in the range of 40 to 200 MPa depending on friction time and interlayer thickness. Thinner interlayers could not maintain the increment of strength due to large material depletion. The strength was degraded by the existence of incomplete joint observed at the interface when a thinner interlayer was used. The hardness value for the mild steel part slightly increased toward the joint because of the formation of aluminium-mild steel intermetallic phase but this was not happen in the alumina part. The joint was created through the mechanical interlocking of aluminium-alumina interface and the formation of intermetallic phase across aluminium-mild steel interface.

A preliminary finite element modeling approach has been described for the simulation and analysis of the friction welding process, which makes use of adaptive meshing and advection algorithms using an explicit code (Abaqus). The fully coupled thermal-mechanical FE model, the peak temperature, the fields of temperature, deformation, stresses and strains are successfully analyzed where maximum values are mostly predicted to be around the periphery of the rubbing surface. The combined features of this approach allow the coupled thermo-elasto-plastic response to be obtained, which clearly shows the extent of the thermomechanically affected zone and the temperature profile immediately after the operation is completed. While the predicted overall deformation shapes are reasonable considering the assumptions made, further refinements are needed to obtain flash during the operation. Also more realistic representation of the temperature dependent elastoplastic material behavior would be expected to decrease the predicted temperatures to more realistic values.

Even though the FE model proposed in this study cannot replace a more accurate analysis, it does provide guidance in weld parameter development and enhances understanding of the friction welding process, thus reducing costly and time consuming experimental approaches.

Acknowledgements

The authors gratefully acknowledge the financial support of this work by the Universiti Teknologi MARA (UiTM), Universiti Sains Malaysia (USM) and Ministry of Higher Education, Malaysia.

References

1. Jun-Ding L, Guang-ming Z and Ping X. Joining Reaction-Bonded Silicon Carbide Using Inconel 600 Superalloy. *Journal of Materials Science Letter*. 2003, 22(10):759-761. http://dx.doi.org/10.1023/A:1023768414427
2. Martinelli AE and Drew RAL. Microstructure Development During Diffusion Bonding of a-Silicon Carbide to Molybdenum. *Materials Science and Engineering A*. 1995, 191(1):239-247. http://dx.doi.org/10.1016/0921-5093(94)09633-8
3. Nicholas MG. *Joining Structure Ceramics in Designing Interfaces for Technological Applications*. London: Elsevier; 1989. PMCid:317996.
4. Dawes C. *Joining of ceramics by friction heating and forging*. TWI, 2001.
5. Jones S. *Can ceramics be friction welded to metals?*. The Welding Institute (TWI), 2003.
6. Brokmeier H-G, Lenser S, Ventzke A, Rotkirch V and Wroblewski T. *Local phase analysis in the welded seam of a FW Al7020/Ti6Al4V sample*. VCH, Wiley; 2008.
7. Meier A, Javernick DA and Edwards GR. Ceramic-metal interfaces and the spreading of reactive liquids. *JOM*. 1999; 44-47. http://dx.doi.org/10.1007/s11837-999-0209-1
8. Taban E, Gould JE and Lippold JC. Dissimilar friction welding of 6061-T6 aluminum and AISI 1018 steel: Properties and microstructural characterization. *Materials and Design*. 2010; 31(5):2305-2311. http://dx.doi.org/10.1016/j.matdes.2009.12.010
9. Fuji A. Friction welding of AlMgSi alloy to NiCrMo low alloy steel. *Science and Technology of Welding & Joining*. 2004; 9(1):83-89. http://dx.doi.org/10.1179/136217104225017166
10. Fukumoto S, Tsubakino H, Okita K, Aritoshi M and Tomita T. Amorphization by friction welding between 5052 aluminum alloy and 304 stainless steel. *Scripta Materialia*. 2000, 42(8):807-812. http://dx.doi.org/10.1016/S1359-6462(00)00299-2
11. Zimmerman J, Wlosinski W and Lindemann ZR. Thermo-mechanical and diffusion modelling in the process of ceramic-metal friction welding. *Journal of Materials Processing Technology*. 2009; 209(4):1644-1653. http://dx.doi.org/10.1016/j.jmatprotec.2008.04.012
12. Frigaard O, Grong O and Midling OT. A process model for friction stir welding of Age hardening aluminum alloys. *Metallurgical and Materials Transactions A*. 2001; 32A:1189-1200. http://dx.doi.org/10.1007/s11661-001-0128-4
13. Avallone E and Baumeister T, editors. *Mark's Standard Handbook for Mechanical Engineers*. 9th ed. Hardcover, McGraw-Hill Companies; 1987.
14. Awang M, Mucino VH, Feng Z and David SA. Thermo-Mechanical Modeling of Friction Stir Spot Welding (FSSW) Process: Use of an Explicit Adaptive Meshing Scheme. In: *Proceedings of the SAE 2005 World Congress & Exhibition*; 2005; Detroit, Michigan. SAE International; 2005. p. 1-6. http://dx.doi.org/10.4271/2005-01-1251
15. Saiz E, Tomsia AP and Sagunuma K. Wetting and Strength Issues at Al/alpha-Alumina Interfaces. *Journal of the European Ceramic Society*. 2003; 23:2787-2796. http://dx.doi.org/10.1016/S0955-2219(03)00290-5
16. Yilmaz M, Çöl M and Acet M. Interface properties of aluminum/steel friction-welded components. *Materials Characterization*. 2002; 49(5):421-429. http://dx.doi.org/10.1016/S1044-5803(03)00051-2
17. Rathod MJ and Kutsuna M. Joining of Aluminum Alloy 5052 and Low-Carbon Steel by Laser Roll Welding. *Welding Journal*. 2004, 83(1):16S-26S.
18. Soundararajan V. *Thermo-mechanical and microstructural issues in joining similar and dissimilar metals by friction welding*. [Thesis]. Boulevard: Southern Methodist University; 2006.
19. Khandkar MZH. *Thermo-mechanical modeling of friction stir welding*. [Thesis]. Columbia: University of South Carolina; 2005.
20. Seli H, Noh MZ, Ismail AIM, Rachman E and Ahmad ZA. Characterization and thermal modelling of friction welded alumina-mild steel with the use of Al 1100 interlayer. *Journal of Alloys and Compounds*, 2010; 506(2):703-709. http://dx.doi.org/10.1016/j.jallcom.2010.07.047
21. Song M and Kovacevic R. Heat Transfer modeling for both workpiece and tool in the friction stir welding process: a coupled model. *Proceedings Institution of Mechanical Engineers Part B*: Journal of Engineering Manufacture, 2004; 218:17-33. http://dx.doi.org/10.1243/095440504772830174